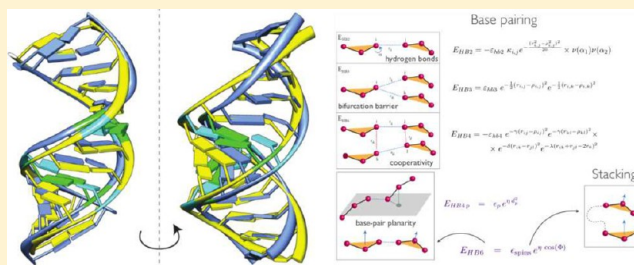


Coarse-Grained Simulations of RNA and DNA Duplexes

Tristan Cragolini,[†] Philippe Derreumaux,^{†,‡} and Samuela Pasquali^{*,†}[†]Laboratoire de Biochimie Théorique UPR 9080 CNRS, Université Paris Diderot, Sorbonne, Paris Cité, IBPC 13 rue Pierre et Marie Curie, 75005 Paris, France[‡]Institut Universitaire de France, 103 Boulevard Saint-Michel, 75005, Paris, France

S Supporting Information

ABSTRACT: Although RNAs play many cellular functions, little is known about the dynamics and thermodynamics of these molecules. In principle, all-atom molecular dynamics simulations can investigate these issues, but with current computer facilities, these simulations have been limited to small RNAs and to short times. HiRe-RNA, a recently proposed high-resolution coarse-grained RNA that captures many geometric details such as base pairing and stacking, is able to fold RNA molecules to near-native structures in a short computational time. So far, it had been applied to simple hairpins, and here we present its application to duplexes of a couple dozen nucleotides and show how with replica exchange molecular dynamics (REMD) we can easily predict the correct double helix from a completely random configuration and study the dissociation curve. To show the versatility of our model, we present an application to a double stranded DNA molecule as well. A reconstruction algorithm allows us to obtain full atom structures from the coarse-grained model. Through atomistic molecular dynamics (MD), we can compare the dynamics starting from a representative structure of a low temperature replica or from the experimental structure, and show how the two are statistically identical, highlighting the validity of a coarse-grained approach for structured RNAs and DNAs.



■ INTRODUCTION

The study of noncoding RNA has been a very active area of research in recent years, as new functions were reported.^{1–5} Many of these RNAs have to fold into specific three-dimensional structures to function in the cell.^{3,6–8}

Despite advances in structure determination, many questions remain open concerning the dynamics and thermodynamics of these molecules. Computational models can complement the experimental data by giving access to the complete atomistic configurations by integration of Newton's equation of motion, using an appropriate force field.⁹ However, the application of such all-atom molecular dynamics (MD) simulations is limited by the considerable computational requirements to integrate such trajectories long enough to sample many folding/unfolding events, even for RNAs containing as little as a dozen nucleotides.¹⁰

In recent years, coarse-grained models have been proposed to alleviate this problem by using simplified representations of biological molecules while striving to keep the important details.¹¹ Such models now exist for both RNA^{12–17} and DNA.^{18–21} The various models reflect the different questions for which they were developed, and no universal coarse-grained model exists. The models differ in the number of beads representing the nucleotides, i.e., in the level of resolution, in the presence or absence of constraints that impose bounds or secondary structures, and even in the shape of the beads, that can go from spherical to elliptical.

HiRe-RNA is such an empirical coarse-grained model for RNA, whose resolution is high enough to preserve many important geometric details, such as base pairing and stacking,²² without imposing preset pairings for the nucleotides. The resolution level, the absence of constraints, and the full flexibility make HiRe-RNA suitable to study folding and unfolding events.

A rigorous way to construct a coarse-grained model would be to start from the atomistic description of the system and integrate over the fast degrees of freedom. This is a bottom-up approach. We have chosen instead to proceed in an empirical fashion, describing the system with simple functions that are chosen to mimic the molecule behavior directly at the resolution scale of the coarse-grained model. The reason for this choice is twofold. On one hand, atomistic potentials for nucleic acids are not yet as well established as they are for other systems, like proteins: when comparing simulations of newer versions of atomistic force fields with simulations obtained from previous force fields, the overall molecular behavior can be substantially different.²³ At present, it is unclear if a convergence in atomistic force field for nucleic acids has been reached, and only from a solid atomistic description can one obtain a sensible coarse-grained force field. Moreover, stacking interactions and hydrogen bonds have a non-negligible

Received: January 23, 2013

Revised: April 26, 2013

Published: June 3, 2013



quantum effect that is not properly treated even by an atomistic classical description.²⁴

The second reason is that potentials obtained from a bottom-up approach tend to be more complex than empirical functions. On a practical level, this complicates the task if the goal is to be able to treat large systems with current computational facilities, and even on conceptual grounds, the use of simple functions can be of help in identifying the main driving forces of the molecular behavior.

The first application of HiRe-RNA concerned simple RNA hairpin topologies of a single molecule. This paper presents an improved version of HiRe-RNA and applies it to double stranded RNAs as well as to a double stranded DNA molecule.

For three sets of molecules, we first performed replica-exchange molecular dynamics (REMD) simulations starting from random configurations, computed specific heat curves, and extracted low-energy structures by clustering of the sampled conformations. The most populated clusters at low temperatures were then reconstructed into fully atomistic structures.

To test whether an atomistic simulation based on the structure we obtain via coarse-grained REMD behaves differently from a simulation starting from the experimental configuration, we performed regular atomistic MD using the AMBER99 force field on both reconstructed and experimental structures.

We first present the coarse-grained model, with an emphasis on the changes with respect to the original model presented in ref 22, as well as the reconstruction scheme that allows us to obtain back an atomistic structure. The full model is presented in the Supporting Information. We then present the different molecules we have studied, two RNA duplexes with non-canonical pairings and one DNA duplex. We illustrate the results of REMD for all systems and extract thermodynamic information such as the melting curve as well as the population distribution at various temperatures. Finally, we compare the atomistic simulations for the reconstructed and experimental molecules.

MODEL

Force Field. In our off-lattice HiRe-RNA model, each nucleotide is represented by six or seven beads (Figure 1): one bead for the phosphate - P -, four beads for the sugar - OS', C5', C4', C1' -, one bead for the pyrimidine bases (B1 = C1 and U1), and two beads for the purine bases (B1 = G1 or A1, B2 = G2 or A2). The positions of the B1 and B2 beads coincide with the centers of mass of non-hydrogen atoms in the all-atom rings. The OH group specific to the ribose is not explicitly represented. This feature allows us to extend the model to DNA molecules as well through a geometric reparametrization for equilibrium values of angles and torsions. Our model cannot account for fine structures of the RNA molecule such as sugar puckers, and single minima potentials are used for dihedrals (refer also to additional material). In the model, we can in principle introduce multiple minima for dihedral potentials, but that is beyond the scope of this work. It would be however essential in studying the interconversion between different forms of helices for DNA.

The HiRe-RNA force field is expressed as a sum of local, nonbonded, and hydrogen-bond (H-bond) terms. Local interactions are the usual harmonic terms for covalent bonds, angles, and torsions. Nonbonded interactions are modeled by a modified Lennard-Jones, characterized by a power-law

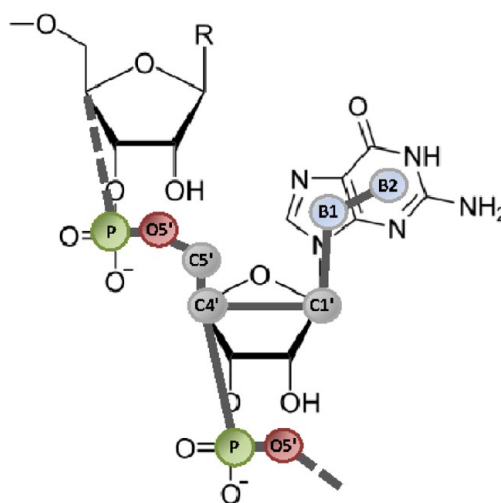


Figure 1. HiRe-RNA coarse-grained representation for a guanine superposed on an all-atom representation.

repulsion core at short distances, a well width changing with the equilibrium distance, and an exponential tail at large distances. Hydrogen bond interactions are specific of our model and consist of three terms: a two-body interaction based on distance and angles between the interacting beads, a three-body term with the role of a repulsion barrier to avoid multiple H-bonds of just one base, and a four-body term of cooperativity involving successive base pairs. The three-body and four-body terms enter in action only when the two-body term reaches significant energies.

HiRe-RNA Version $\beta.2$. Leaving unaltered the local and nonbonded terms presented in ref 22, we have introduced some modifications to the hydrogen-bond terms. H-bonds are clearly the hardest interactions to account for because they are somewhere in between a classical and a quantum interaction. As we apply HiRe-RNA to more and more structures, we are inevitably brought to make changes to ameliorate this term.

The two significant changes we introduced are in the two-body and four-body terms (refer to Figure 2 for the general base-pairing scheme and particle numbering). In the original version of the force field, the distance component of the two-body term was a 5–10 LJ interaction. We have found that the repulsion core of the interaction was sometimes interfering with the stacking of successive base pairs. Given the interaction grows spherically all around the interacting bead, as opposed to being confined on an hypothetical H-bond plane, the repulsion could push away a bead interacting with the successive base. The problem could rise, for instance, in the following scenario. Consider a base i interacting with a base j and a base $i + 1$ interacting with a base $j - 1$. Depending on the overall torsion of the helix, it can occur that the equilibrium distance between i and $j + 1$ is in a range where the repulsion core enters in action. Given that most likely the angular dependence of the energy function is still rather good (since particle $j + 1$ is aligned only a few Å away from j which bonds correctly with i), the dominant effect will be that of repelling base $j + 1$ away from i and therefore stretching the helix. We decided to eliminate the repulsive core from the two-body term of the hydrogen interaction and to make it exclusively attractive. A generic hard core repulsion between all beads in the nonbonded interaction already governs the excluded volume of all particles.

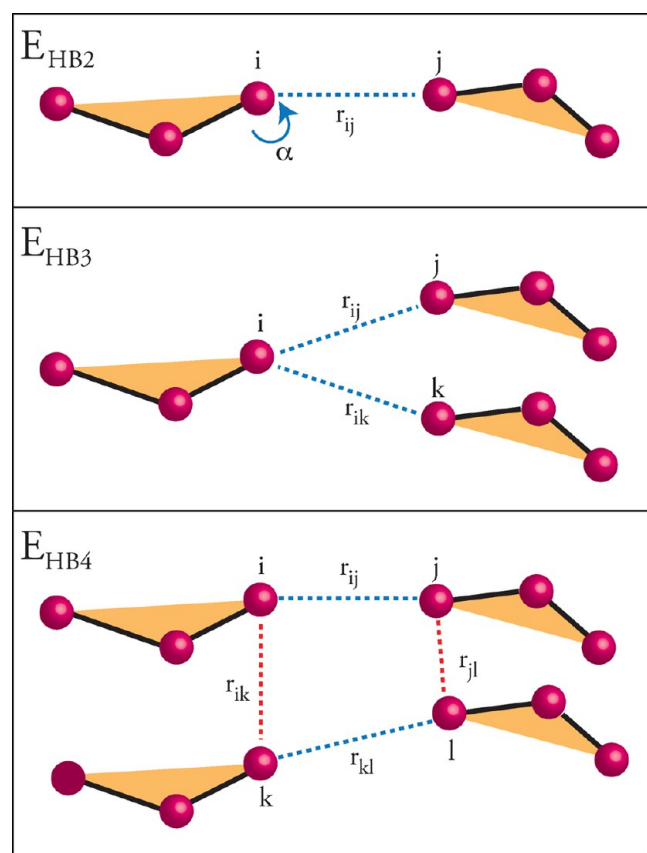


Figure 2. Base pairing is modeled through three different energy terms that depend on the geometric configurations adopted by two (E_{HB2}), three (E_{HB3}), or four (E_{HB4}) bases. For each of these interactions, we indicate the variables upon which the energy term depends.

The distance contribution of the two-body term takes now the simple form of an inverted quartic exponential:

$$E_{HB2} = -\epsilon_{hb2} e^{-\nu(r_{ij}^2 - \rho^2)^2} \quad (1)$$

where ϵ_{hb2} is the strength of the interaction, ν is the parameter regulating the range of the interaction, ρ is the equilibrium distance, and r_{ij} is the instantaneous distance for particles i and j .

The other change we introduced is in the four-body term. In the original version of HiRe-RNA, cooperative effects were calculated only for pairs of successive bases, as in the case of i being bound to j and $i + 1$ to $j - 1$. It can happen however that two base pairs are stacked on top of each other and therefore have a cooperative stabilization effect, even if they are not successive along the chain. This is typical of junctions where two helices can be perfectly stacked on top of each other to the point of forming a seemingly continuous helix like in tRNAs and in many other large RNA molecules.²⁵ We modified the function to take into account only the geometric placement of the two base pairs with respect to each other, and not their sequentiality. Consider base i bound to base j and base k bound to base l , with base k stacking to base i and base l stacking to base j . The interaction energy is composed of four Gaussians:

$$E_{HB4} = -\epsilon_{hb4} e^{-\gamma(r_{ij} - \rho_{ij})^2} e^{-\gamma(r_{kl} - \rho_{kl})^2} e^{-\delta(r_{ik} - r_{jl})^2} e^{-\lambda(r_{ik} + r_{jl} - 2r_0)^2} \quad (2)$$

where r_{ij} is the instantaneous distance of particle i and particle j , ρ_{ij} is the equilibrium distance for the specific hydrogen bond (which varies depending on the base nature in the pair), r_{ik} and

r_{jl} are the distances between particle i and particle k and particle j and particle l , respectively, and r_0 is a cutoff distance for the interaction to vanish. In essence, this function gives an additional energy gain if two bonds are formed simultaneously and if the bases are aligned in a “square” configuration.

As a minor change, the three-body function has been simplified from its original form to gain stability and increase code performance:

$$E_{HB3} = \epsilon_{hb3} e^{-\eta(r_{ij} - \rho_{ij})^2} e^{-\eta(r_{ik} - \rho_{ik})^2} \quad (3)$$

where particles j and k are both susceptible to pair with particle i .

All of these changes have been tested on the two benchmark molecules 1EOR and 1N8X used in the original publication. Through MD simulations, the new version $\beta.2$ folds these molecules to their NMR structures within 2–3 Å.

Note that we do not use temperature dependent coarse-grained potentials, and this may have an impact on thermodynamics and notably the position of the heat capacity peak. However, even all-atom simulations of proteins in explicit solvent can lead to a shift of 30 K for the melting temperatures.²⁶

The complete description of all energy function, geometric, and energetic parameters is available in the Supporting Information.

Reconstruction Procedure. With the nucleobase being relatively rigid fragments, the full atomic configurations of an RNA molecule can be well described with a small number of internal coordinates, involving mostly the phosphate and sugar moieties.²⁷ Most of this information is preserved in HiRe-RNA’s representation. To obtain a highly accurate reconstruction, we performed a statistical analysis on the RNA structures present in the Nucleic Acid Database (NDB),²⁸ and determined which internal coordinates explicitly represented in our model most strongly correlate with the missing degrees of freedom. Using this information, we are able to reconstruct high-quality all-atom structures of RNAs from a corresponding coarse-grained representation.

Using the RNA conformer data presented in ref 27, we selected a number of prototypes, expressed in internal coordinates, representing the most common motifs present in RNA (helix, loop, and turn). Given the bond lengths, angles, and torsions of a coarse-grained nucleobase, we can choose the best suitable atomistic prototypes, and convert the internal coordinates into atom positions.²⁹ This procedure is repeated for each residue (see Figure 3). The overall scheme is particularly efficient given it uses neither a fragment search nor an optimization procedure.^{30,31}

We validated our reconstruction procedure on 146 structures extracted from the PDB. For each experimental structure, we first generated the coarse-grained model and then, from this, reconstructed the fully atomistic structure. We compared the experimental structure and the reconstructed structure by computing the RMSD on all atoms. The RMSD between the original and reconstructed structures has a mean of 0.18 Å, with a maximum value of 0.516 Å, values that are well below the resolution of most crystallographic data on biomolecules. This is a clear indication that the reduction scheme of HiRe-RNA well preserves the geometric information of an RNA conformation.

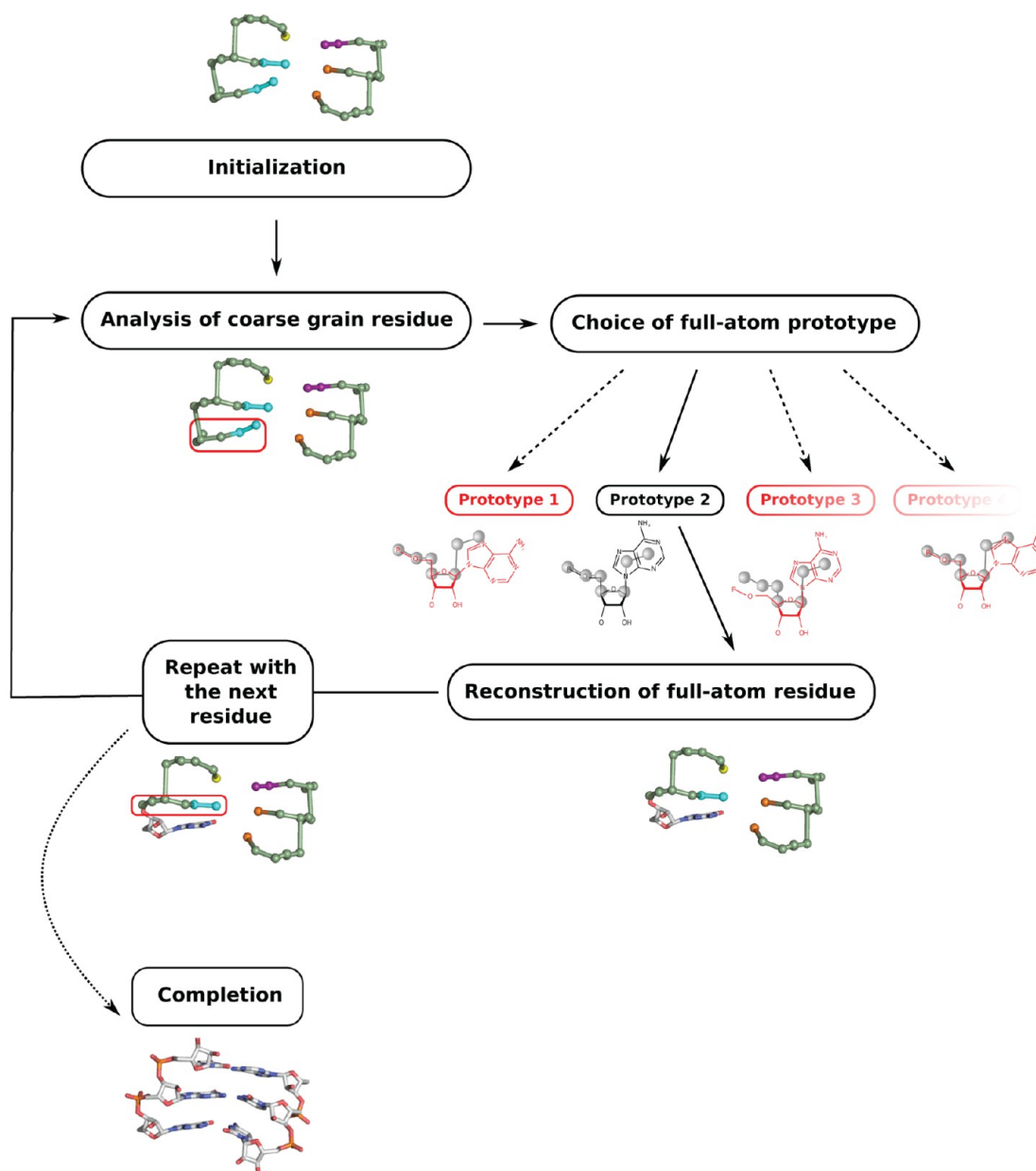


Figure 3. Schematic of the reconstruction method used to convert from a coarse grain to an all-atom structure.

SYSTEMS

We investigate here molecules of size similar to the one presented in the original paper of HiRe-RNA but with different topologies. We have chosen two RNA duplexes of a total of 32 and 36 nucleotides each that adopt a double helical structure and one DNA duplex of 24 nucleotides in total. Both RNA double helices contain non-canonical base pairings, A·C in one case and G·U in the other. Figure 4 shows the sequence and base pairing of all duplexes. We studied also a DNA double helix in the B-form, therefore a significantly different helix from the one formed by typical RNA, which adopts an A-form.

RNA Double Helices. The two double helices are the “structure of a 16-mer RNA duplex with wobble C·A mismatches”, PDB code 405D,³² and the “structure of a 14 bp RNA duplex with non-symmetrical tandem G·U wobble base pairs”, PDB code 433D.³³

The sequence of 405D is $r(\text{GCAGACUAAAUCUGC})_2$ and its crystal structure has been resolved at 2.5 Å resolution³²

(Figure 5A). It is characterized by two wobble A·C pairs, between C6 and A27 and between A11 and C22, respectively. All other bases form canonical Watson–Crick (WC) pairs. The presence of the mismatch alters the width of the grooves and provides a possible recognition site for proteins. A·C mismatches are more rare than wobble G·U pairings, but they are biologically important, as they replace G·U pairs in rRNA and are found in some codon recognition of tRNAs.

The sequence of 433D is $r(\text{GGUAUUGCGGUACC})_2$ and its crystal structure has been determined at a 2.1 Å resolution³³ (Figure 5B). This duplex contains two successive nonsymmetrical G·U wobble base pairs, which deform significantly the helix with respect to a regular A-helix. A full description of these differences is given in the section concerning the comparison of 433D and 433Dsym. This deviation from the canonical RNA helix shape could play the role of a sequence-specific recognition site. Comparisons of rRNA sequences have shown that non-symmetrical tandem mismatches with the

| | | |
|---------|--|--------|
| 405D | 5'- G C A G A C U U A A A U C U G C - 3' 3'- C G U C U A A A U U C A G A C G - 5' | 16 x 2 |
| 433D | 5'- G G U A U U G C G G U A C C - 3' 3'- C C A U G G C G U U A U G G - 5' | 14 x 2 |
| 433Dsym | 5'- G G U A U U G C U G U A C C - 3' 3'- C C A U G U C G U A U G G - 5' | 14 x 2 |
| 3BNA | 5'- C G C G A A T T C G C G - 3' 3'- G C G C T T A A G C G C - 5' | 12 x 2 |

Figure 4. Base pairing schemes for each one of the systems analyzed. For 433Dsym in blue are the bases exchanged with respect to the wild form 433D.

sequences 5'-U-U-3'/3'-G-G-5' are much less frequent than the symmetrical motif 5'-U-G-3'/3'-G-U-5' in all kinds of secondary structure environments.³⁴ Experimentally, it is also observed that the non-symmetrical mismatch alters the stability of the molecule with respect to an all WC helix.³³ It has been reported from optical melting studies on duplexes with eight nucleotides on each strand that the non-symmetrical mismatch G-U increases the stability by 1 kcal/mol with respect to the symmetric motif 5'-U-G-3'/3'-G-U-5'.^{33,35} To investigate the stability of the symmetrical mismatch with respect to the non-symmetrical wild form, we created a new molecule, not studied experimentally, named 433Dsym, in which we have inverted one of the G-U mismatches to obtain the symmetric motif.

DNA. In our model, there is no explicit representation of the OH group, since the sugar is represented by the C5'-C4'-C1' particles, and therefore, we do not distinguish the ribose from the deoxyribose. The only changes we need to introduce in order to study DNA molecules are equilibrium values of the geometric parameters governing angles and torsions, which differ from RNA, and the relative values of the energy of base

pairings to keep into account that DNA couples almost exclusively through Watson-Crick G-C and A-T. We apply our model to a DNA double helix of size similar to the RNA duplexes. The details of the differences between RNA and DNA are given in the Supporting Information. Geometric parameters were taken from the standard values of B-DNA on the NDB. We have chosen to study the 3BNA duplex,³⁶ which is a reference for B-DNA helix and whose size is of 12 nucleotides on each strand.

The sequence is r(CGCGAATTCGCG)₂ (Figure 5C). Major and minor grooves are clearly distinct, as typical for a B-helix, in contrast with an A-helix, where the two grooves are more similar in width.

COARSE-GRAINED SIMULATION

For all molecules, we ran a set of replica exchange molecular dynamics (REMD)³⁷ using a Langevin thermostat.³⁸ This is an enhanced sampling method allowing to sweep over several temperatures at once. A preset number of molecular dynamic (MD) simulations are run simultaneously at different temperatures, and at fixed time intervals, a swap between configurations of neighboring temperatures is attempted and accepted or rejected based on the Boltzmann probability calculated on the energy difference of the two configurations.³⁹ In practice, at the swapping time, the energies of two replicas are compared and if the replica at the higher energy has an internal energy lower than that of the lower temperature replica, the exchange between the two configurations is always accepted. In the opposite case, the exchange is accepted based on a Metropolis criterion. This procedure is carried out using a protocol recently presented in ref 40 where a multitude of Monte Carlo steps in attempted replica swapping are performed at each preset time. This approach results in a great enhancement of the sampling while not altering the final statistical distributions of measurable quantities.

Given that the force field of HiRe-RNA has not yet been optimized, the absolute strengths of the interactions do not reflect experimental values and only relative strengths are relevant. Our temperature therefore loses for the moment its connection with the real temperature and is expressed in terms of an arbitrary scale Θ .

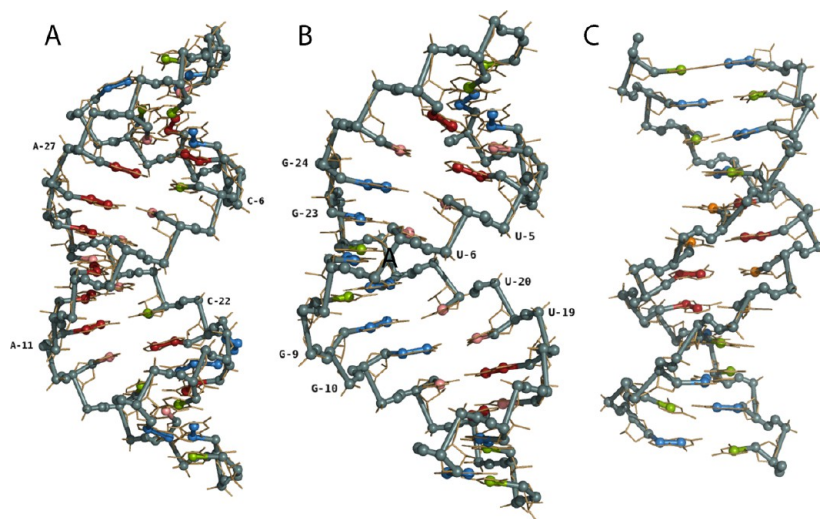


Figure 5. The coarse-grained representation of three duplex systems superposed to the fully atomistic structures: 405D RNA (A), 433D RNA (B), 3BNA DNA (C). (Base color coding: dark red, A; pink, U; orange, T; green, C; blue, G.)

General Simulations Protocol. For each duplex, we generated REMD trajectories from a completely unfolded state. This starting point was taken from a snapshot of a long simulation at high temperature starting from the experimental structure. The configurations taken as the unfolded states all consist of two unpaired strands at an average distance comparable to the single strand length, and no interstrand hydrogen bonds.

All simulations are carried out with spherical bounds of radius 65 Å, while the strand extension is between 70 and 60 Å for all molecules. This relatively high concentration was chosen to minimize the encounter time of the two strands, which is basically a random walk in 3D, and can be the most time-consuming (and uninteresting) part of the simulation.

The REMD consists of 24 replicas with temperatures in units of Θ .

For the double helical RNA systems, the temperatures are the following: 220.0, 235.0, 246.677, 255.463, 264.563, 273.987, 283.746, 287.0, 290.0, 293.853, 297.0, 300.0, 302.0, 304.320, 308.0, 312.0, 315.160, 320.0, 326.386, 330.0, 338.011, 350.051, 362.433, 380.0.

For the DNA system, the temperatures are the following: 215.00, 230.00, 250.000, 262.818, 276.293, 290.459, 305.351, 321.006, 337.465, 345.00, 354.767, 362.00, 372.956, 377.00, 382.00, 387.00, 392.078, 397.00, 402.00, 412.180, 433.313, 455.530, 470.00, 490.885.

These values were chosen after several trial runs, in which we made sure to have an adequate exchange between replicas and a sufficient temperature range to include the specific heat peak with a good margin on both sides. Each replica was simulated between 100 and 600 ns, and the overall internal energy monitored. In the analysis, we included only the portions of simulation where the internal energy had reached stability. The convergence of the simulation is verified by the superposability of the thermodynamic properties computed separately on different portions of the simulation on one hand, and by the number of full excursions of the replicas on the entire temperature range on the other. For the analysis, we monitored the number of native base pairs and the overall RMSD from the experimental structure. A base pair is considered formed if the bonding two-body energy is at least half of its maximal theoretical value, based on the energy function we have defined, i.e., $|E_{\text{HB2}}(\text{bond})| \geq \frac{1}{2}|E_{\text{HB2}}(\text{max})|$. All conformations were clustered recursively as follows: after computing the RMSD between all pairs of structures, we identify the structure with the largest number of neighbors using a cutoff of 2.5 Å; the center and all members of this cluster are removed, and the procedure is repeated until all states are clustered. Finally, thermodynamic properties were extracted from REMD simulations using the weighted histogram analysis (WHAM).⁴⁰

For a molecule of 22 nucleotides, it takes 25 s per nucleotide per simulated nanosecond on an Intel 3.0 GHz processor. That is, it takes 9 min to simulate 1 ns and 8 h for 50 ns.

RESULTS

For each REMD, we have determined the specific heat curve, in which we can observe the thermodynamical transition of assembly/dissociation of the duplex. We have performed a cluster analysis of structures at each temperature to determine the most populated configurations. Combining these two analyses allows us to draw the full picture of the molecule behavior at various temperatures.

In principle, if we only consider the energy of base pairing, we could expect a situation where low temperatures are dominated by duplexes, since they maximize the number of pairings, and therefore minimize the internal energy, intermediate temperatures where the two strands are dissociated but folded, and the melted state, where the strands are both dissociated and free-floating. However, for all molecules, we find very neat assembly curves for the duplex with only one peak corresponding to the assembly transition, while we never see hints of the presence of two separately folded single strands.

405D. Figure 6 shows the specific heat curve for 405D obtained from a 100 ns simulation. The first 30 ns were

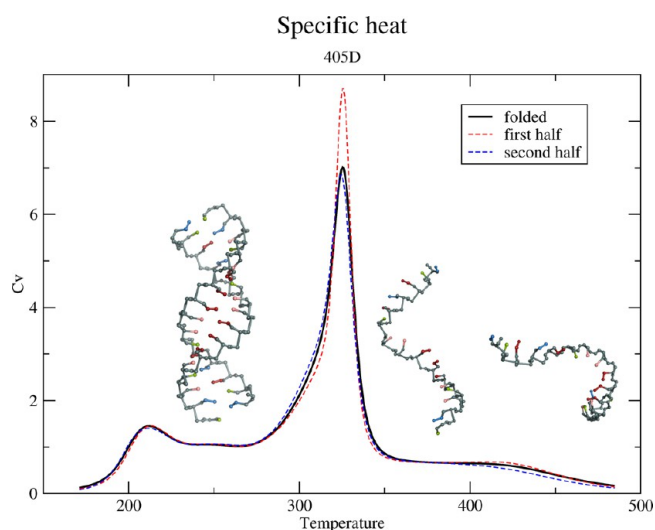


Figure 6. Specific heat curve for 405D. The black curve is obtained for the whole trajectory having excluded the first 30 ns of the simulation. The two colored curves are obtained by considering the first half of the simulation (30–65 ns: red) and second half (65–100 ns: blue), respectively, and by their superposition show the good convergence of the simulation. On the left of the peak, the structure of the most populated structure at T3 (247 Θ) and on the right a representative configuration at high temperatures, T22 (350 Θ).

excluded from all analysis. We can observe the good convergence of the simulation as verified by the superposability of the curve if we consider only half of the trajectory at the time. To further assess the good convergence of the simulation, we also monitored the migration of each replica over all temperatures, and we observed that each replica makes several dozens of full temperature excursions in the simulated time.

The system exhibits a single melting transition at 325 Θ , with no hints of the possible presence of two folded hairpins. Below the melting temperature, the native duplex structure is dominant, while above it the two strands are fully unfolded and behave independently. In principle, because of the base complementarity, each single strand could fold back on itself to form a hairpin with a tetraloop, each stem still containing one of the two mismatches present in the duplex. The structures of the single strands for these duplexes are not known, but starting from a single strand random configuration, we can obtain the structure of a folded hairpin. We then ran REMD simulations from an unpaired state where the two single strands were folded upon themselves, forming two stable hairpins. This was done to test whether the double helix is indeed the most stable structure and to rule out that the duplex might be a very long-lived metastable state. Indeed, we find that in the temperature

range of the duplex melting transition, and at our concentrations, the folded hairpins open and reform the duplex. We can then conclude that the duplex is the preferred configuration both energetically and entropically at the concentrations we are simulating, and that only by significantly increasing the dilution we could observe stable hairpins. Other systems exhibit the duplex configuration as the most stable structure. This is the case, for example, for the kissing loop system, where the configuration of the two hairpins connected by a loop can be a metastable state leading to an extended, functional duplex.⁴¹

433D, 433Dsym. For these two systems, our main question is whether or not we are able to capture the thermodynamic differences between the symmetric and antisymmetric tandem G·U mismatch. We expect these differences to be very subtle, and we therefore need to cumulate very large statistics. The two systems were simulated in three independent sets of REMDs of 600 ns each, and only the last 300 ns of each simulation were used to compute statistics. Two of the simulations were started from unfolded configurations only, and one was started from a mixture of unfolded and folded initial configurations. The specific heat curves are shown in Figure 7 for each system. For

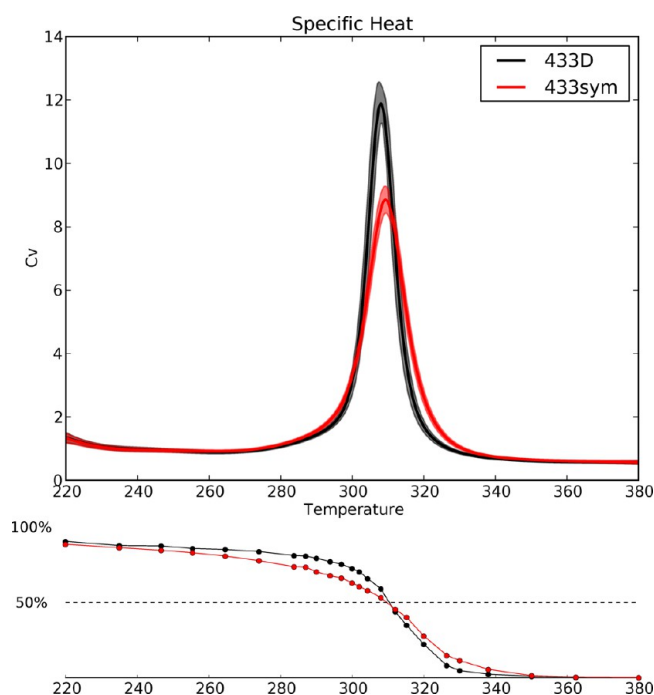


Figure 7. Top: Specific heat curve for 433D (black) and 433Dsym (red). The shaded area around the middle line represents the uncertainty of the measure calculated with the bootstrap method. Bottom: Percentage of folded structures for the two systems as a function of simulation temperature.

each curve, we represent both the mean C_v curve as well as its error computed using a boot strap method to obtain a width of the curve representative of the uncertainty. For each temperature, we also measure the overall percentage of folded structures for each system defined as the percentage of structures with an RMSD relative to the experimental structure of less than 4 Å. The two C_v peaks are superposable, and if there are small temperature differences in their exact position, they are well within our uncertainty.

Although we cannot distinguish the two systems based on the positions of the specific heat peaks, we observe significant differences in the width of the peaks, with the peak of 433D more pronounced and narrower than the peak of 433Dsym. This implies that 433Dsym has a transition over a wider temperature range than 433D. The difference in the width at half-maximum for the two peaks is of the order of 10 K, which is above our uncertainty estimated at a few K.

This observation is also supported by the data on the percentage of folded structures. 433Dsym has a lower proportion of folded structures than 433D at $T < T_m$, but it has a higher proportion of native structures at $T > T_m$. This suggests that 433D has a more cooperative transition than 433Dsym: at the melting temperature, 433D is more sensitive to thermal fluctuations than 433Dsym.

To further investigate the thermal stability of the two molecules, we have computed the potential of mean force (PMF) of each structure relative to the native RMSD and the number of hydrogen bonds, at temperature close to T_m (Figure 8). PMFs are built using WHAM at any given point in the

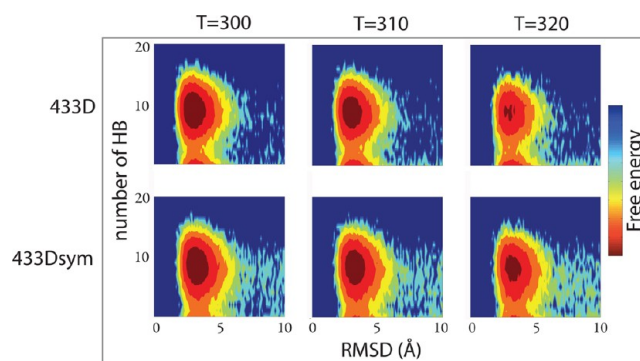


Figure 8. PMFs of 433D (top) and 433Dsym (bottom) with respect to the native RMSD and to the number of paired bases. The potentials of mean force (PMF) are computed at different temperatures close to T_m . At high temperatures, a second basin at ~ 25 Å, corresponding to unfolded structures, appears. For image clarity, it is not shown here.

chosen coordinate space. For both systems, we notice a large free energy minimum at 3 Å RMSD centered around 10 base pairings. At 300 K, the basins of attraction of the free energy minima are very similar, with that of 433Dsym expanding slightly more toward higher RMSD. As the temperature increases, the depth of the minima diminishes, and states at higher RMSD are populated (not shown in the picture). We notice that as the temperature increases the basin of 433Dsym remains deeper and wider compared to 433D. We can then compute the percentage of structures belonging to the basin for each system at the various temperatures. At 300 K, for both molecules, 97% of all structures belong to the PMF basin. At 310 K, 68% of all 433D structures fall into the basin, while they are 75% for 433Dsym. At 320 K, the discrepancy increases further with only 25% of 433D versus 43% of 433Dsym. Our findings suggest a greater thermal stability of the sequence containing the symmetrical mismatch. This result, although rather qualitative, is in agreement with the experimental evidence on tandem G·U motif stability.³⁵ We can therefore conclude that, despite our inability of detecting differences in the specific positions of the melting peaks, we can still capture significant differences in the molecules' thermodynamic behavior.

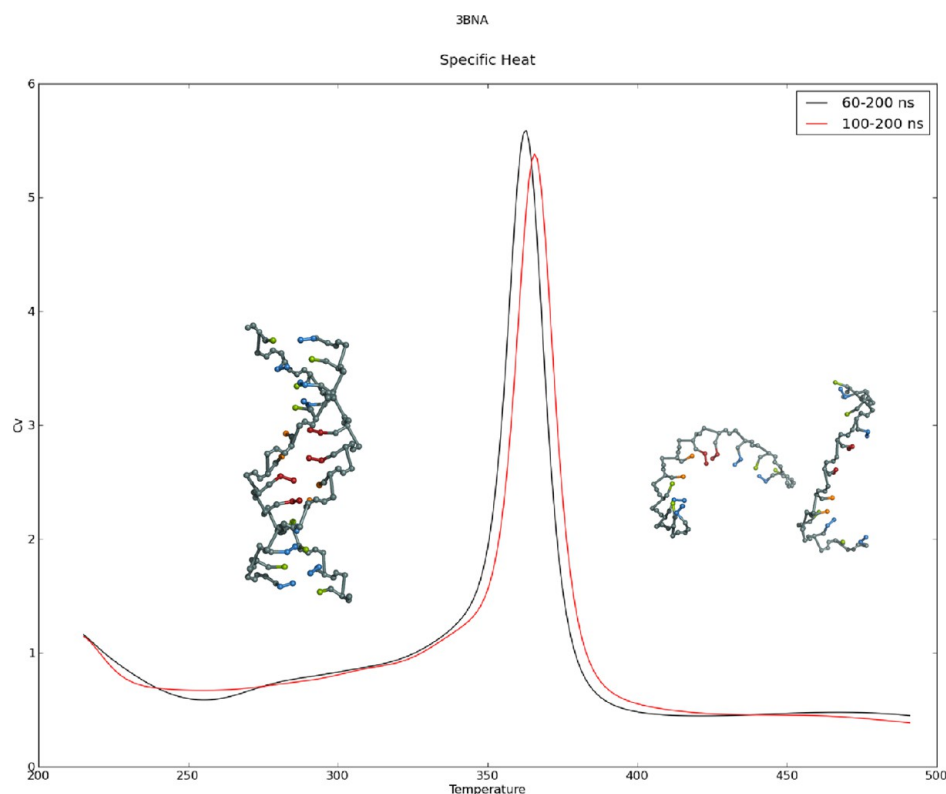


Figure 9. Specific heat curve for 3BNA. The representative structure at temperatures below the melting peak is the most populated cluster at T7 (305 Θ). Its n-RMSD is 2.7 Å, and all native base pairs are correctly formed. As we can visually observe, the major and minor grooves are clearly distinct as it should be for an A-form helix.

3DNA. For the DNA system, the specific heat curve is shown in Figure 9. As for the RNA systems, we observe a very neat transition, characterized by one single peak corresponding to a melting transition. We can observe that the DNA molecule melts at higher temperatures than the RNA duplexes. This is expected from the base content of the DNA where all base pairs are canonical WC couplings.

Cluster analysis shows the presence of a single dominant cluster at low temperatures with the correct native base pairing, and with an RMSD of 2–3 Å from the experimental structure. The cluster gradually drops in population approaching the melting peak.

Energy Scale. Given that our model is empirical (it does not come from an integration procedure), the only way to establish an energy scale is to compare our melting temperature results with experiments. This is an ongoing project at our institute, where experimentalists will provide us with melting curves for duplexes we can simulate. In the meantime, we can get an estimate of the energy scale by comparisons with algorithms that compute melting temperatures. HyTher^{42,43} is such an algorithm which has also been used in the parametrization of other coarse-grained models.¹⁸ The comparison of melting temperatures obtained from our specific heat curves with those predicted by HyTher is given in Table 1. Our predicted melting temperatures are in good qualitative agreement with those calculated by HyTher, with the correct ranking and proportionate temperature gaps between the various systems. Concerning the quantitative values, we would be inclined to say that our units of Θ correspond to degrees K. This 1:1 correspondence is also suggested considering that H-bonds in our energy scale average between 3 and 4 (depending

Table 1. Comparison of Melting Temperature Prediction between HiRe-RNA and HyTher

| molecule | HyTher | HiRe-RNA |
|----------|--------|---------------|
| 405D | 328k | ~330 Θ |
| 433D | 293k | ~310 Θ |
| 433Dsym | 291k | ~310 Θ |
| 3BNA | 348k | ~360 Θ |

on the base content and orientation) while experimental values are about 3 kcal/mol.

■ ATOMISTIC SIMULATIONS

The main goal of atomistic simulations on our systems is to compare the behavior of simulations starting from experimental structures with simulations starting from structures reconstructed from coarse-grained predictions. If the two sets of simulations compare well, we are then justified to use the coarse-grained model to perform folding and assembly simulations of molecules for which the native state is unknown, and then refine the results via atomistic simulations. We use this approach to study the structural differences of 433D and 433Dsym at the atomistic level.

For the three double strand systems for which the experimental structure exists (405D, 433D, and 3BNA), the reconstruction is carried out following the procedure outlined earlier from a low temperature equilibrium configuration of the REMD simulations. To verify if the simulations from the experimental structure and the corresponding reconstructed structure are comparable in general behavior, we monitor the time evolution of the RMSD with respect to the experimental structure, computed on all heavy atoms of all internal

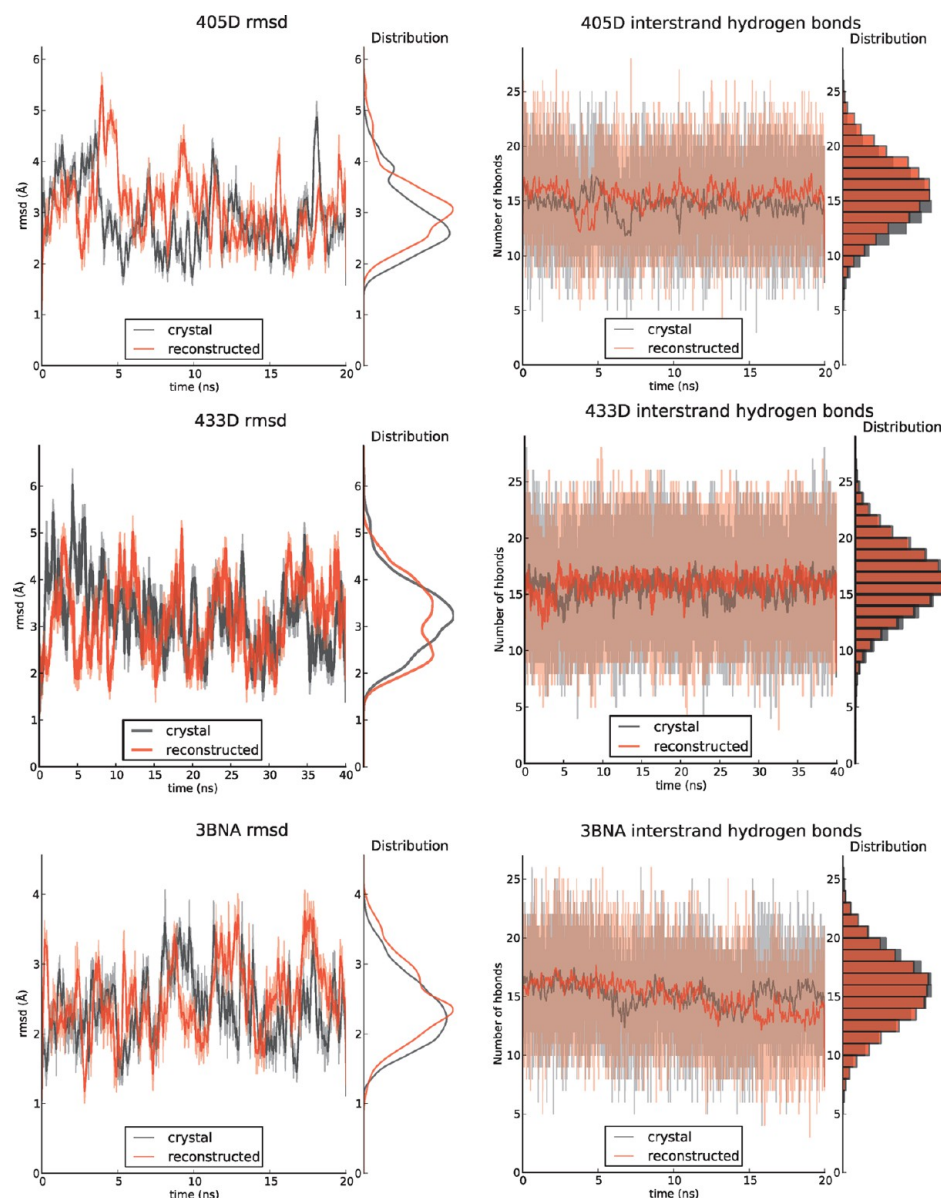


Figure 10. Time series and distributions of n-RMSD and interstrand hydrogen bonds for each atomistic system in the two sets of simulations, from the experimental structure and the reconstructed structure. The error on the distribution of the RMSD is estimated to be 0.5 Å. This is obtained from the analysis of the first half of the trajectory and the second half of the trajectory taken separately and then compared.

nucleotides (i.e., excluding from calculations the first and last nucleotide of each chain), the time evolution of the number of interbase hydrogen bonds, and we compare the distributions of the most populated clusters. Hydrogen bonds are calculated with the program VMD⁴⁴ with the criteria of a donor–acceptor distance of less than 3 Å and of an angle of less than 20°. Since the instantaneous number of hydrogen bonds is subject to large fluctuations, due to the sharp definition used in calculating the presence of a bond, we compute instead a running average over a 100 frames and use this quantity for the comparisons between the two simulations. Clusters are computed using the gromacs⁴⁵ program *g_cluster* with a cutoff of 2 Å.

All-Atom Reconstructed Molecules. First, we compare the starting structures for the simulations. For each system, we have four possible structures: the experimental crystal structure (C), the experimental structure relaxed after thermalization (CX), the reconstructed structure (R), and the reconstructed structure after thermalization (RX). When we consider the

reconstructed structure R in comparison with C, the RMSDs are low (2.7 Å for 3BNA, 2.5 Å for 433D, and 3.7 Å for 405D), but we notice a significant discrepancy in the number of interbase hydrogen bonds (405D rx, 18; 405D rec, 4; 433D rx, 19; 433D rec, 3; 3BNA rx, 13; 3BNA rec, 7). This suggests that some of the bases of the reconstructed structures are not well aligned despite the general shape of the molecule being very similar. We also notice that none of the crystal structures have a number of interbase hydrogen bonds close to the value one would expect in theory adding the number of bonds of each kind of base pairs (2 for AU, GU, and AC when considering a WC/WC binding and 3 for GC). The number of interbase hydrogen bonds is around 50% for all systems instead.

When we look at the relaxed structures, all major differences disappear. RMSDs for all three systems are lower (2.6 Å for 3BNA, 1.8 Å for 433D, and 2.8 Å for 405D), and the number of hydrogen bonds differs by at most five bonds (433D), which accounts for 15% of all possible bonds. It is then clear that

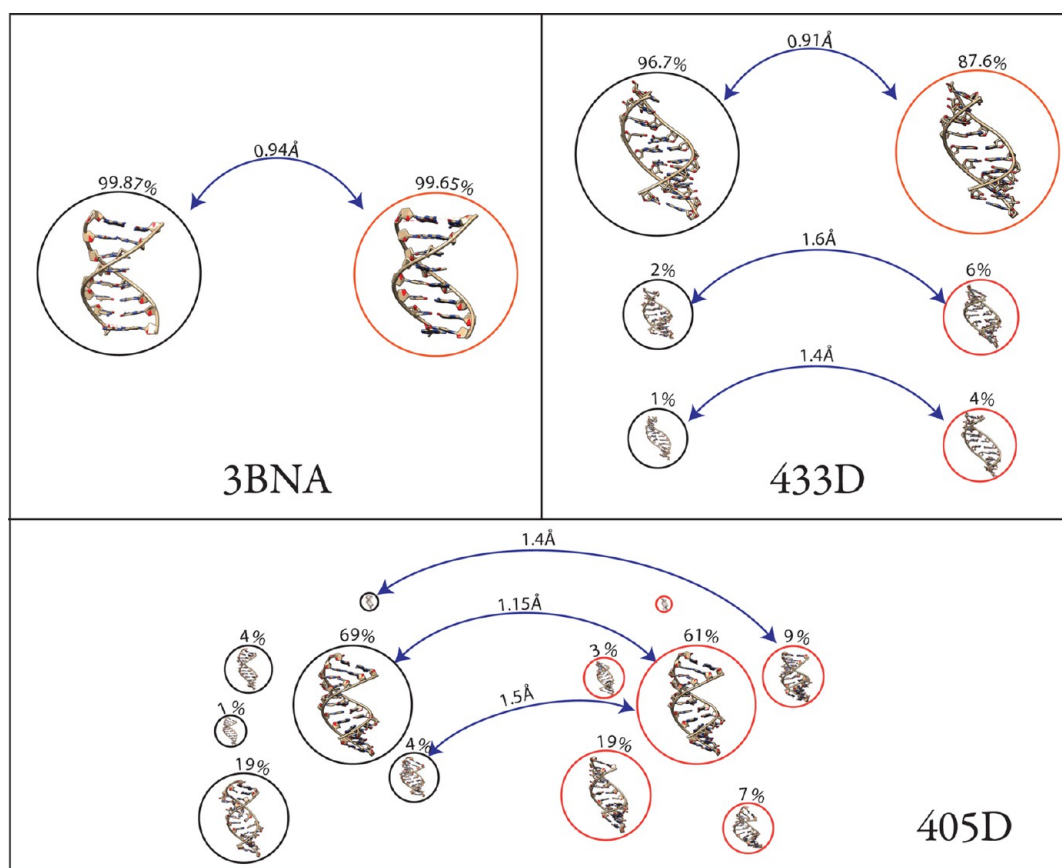


Figure 11. Cluster comparisons between the E-sim (black) and the R-sim (red) for the three systems. The percentage on top of each cluster indicates the relative cluster population, and the arrow between a black and a red cluster indicates the RMSD between corresponding clusters in the two types of simulations, measured from the cluster centers.

comparisons are meaningful only on relaxed structures for both the experimental and reconstructed configurations.

All-Atom Simulations Protocol. For all-atom simulations, we used the parmbsc0 forcefield⁴⁶ as implemented in amber 11. We used the TIP3P model for water,⁴⁷ and the long-range electrostatic interactions were treated with the particle mesh Ewald method, using a 10 Å real space cutoff. SHAKE was used to constrain all bonds involving hydrogen atoms, and a 2 fs time step was used. The temperature was kept at 300 K using a Langevin thermostat and a 5 ps⁻¹ collision frequency. Pressure coupling used the Berendsen algorithm with isotropic position scaling and a relaxation time of 2 ps. The target pressure was kept at 1 bar.

All simulations were done using the same protocol:

- The system's charge was neutralized by adding Na⁺ ions.
- A truncated octahedron box was used, with a minimal buffer distance of 10 Å between the box's boundary and the RNA molecule. Water molecules using the TIP3P model were then added to the box.
- The system was then subjected to energy minimization.
- A short MD run of 0.2 ns was used, with restraints on the solute, in order to equilibrate the solvent, and the soft restraints used on the solute allowed reconstructed structures to relax to more stable states, i.e., better stacking of neighboring bases, and improved orientation in a base pair.
- With all restraints removed, we did a thermal equilibration, followed by pressure equilibration for a total of 0.8 ns.

- Finally, the production simulations were run for 20 ns in the NPT ensemble for 405D, 433Dsym, and 3BNA and 40 ns for 433D.

Experimental vs Reconstructed Structure MD. For all three systems, we are now going to compare atomistic MD simulations ran starting from the experimental structures (E-sim) and simulations ran from the reconstructed structure (R-sim) obtained from the most populated low temperature cluster of the coarse-grained simulation, for the two RNA double helices 405D and 433D and for the DNA 3BNA.

All three sets of simulations exhibit a very similar behavior when starting from the experimental structure and from the reconstructed structure. We observe no significant qualitative difference in neither the time evolution of the RMSD nor the number of interbase hydrogen bonds. This can be observed also from a comparison of the respective distributions of these two quantities over the whole simulation, which are superposable for the number of interbase hydrogens, and have peaks centered around the same values for the RMSD (Figure 10). In both E-sim and R-sim, the number of window-averaged interbase hydrogen bonds (IBHB) fluctuates at three or four bonds around the mean value (i.e., a fluctuation of about 20% with respect to the average number of bonds present during the simulation, or of 10% of the overall possible number of bonds), while the instantaneous values vary much more significantly, with fluctuations of the same order as the mean value. This is also in part due to the sharp cutoff used to evaluate the presence of a hydrogen bond. For example, the crystal structure of 405D is characterized by 21 hydrogen bonds between the

bases, but throughout the simulation, the number of instantaneous IBHB fluctuates symmetrically around the mean value of 16, spanning from as little as 6 to a maximum of 27. A very similar result is obtained from the reconstructed structure with a mean value of IBHB of 16 as well, a lowest value of 3 and a highest value of 25. Similar results are found for the other two systems, as shown on the right-hand side of Figure 10. However, the overall shape of the molecule does not change significantly, as shown by values of RMSD with respect to the experimental structure that rarely go above 5 Å (left-hand side of Figure 10). In the time span of our simulations, what we observe are possible local rearrangements of the bases, that can slightly bend and/or rotate about their plane and about the backbone.

For both E-sim and R-sim, we notice that the RNA duplexes show more variability than the DNA duplex. Clustering analysis shows only one significant cluster for the DNA system (native, 99.8%; reconstructed, 99.6%), while, for the RNA systems, one cluster is clearly dominant, but other smaller clusters are also present (Figure 11). The most populated cluster of 433D is at 96.6% for the native simulation and at 87.6% for the reconstructed simulation, and that of 405D is at 69.2% for the native simulation and at 61.3% for the reconstructed one. When we compare the clusters for both sets of simulations, we see that in all instances the most populated cluster found in the native state simulations corresponds to the most populated cluster of the reconstructed simulation, as it is shown by crossed RMSDs of about 1 Å, while the clustering is performed using a 2 Å cutoff. For 3BNA, only one cluster is present in both simulations and the centers of the clusters are 0.94 Å apart. For 433D, the centers of the most populated clusters on both simulations are 0.91 Å apart. The other, less populated clusters have a clear correspondence between the two simulations, with the second most populated cluster of one simulation exhibiting the lowest RMSD with the second most populated cluster of the other simulation (1.6 Å), and the same happening also for the third most populated clusters (1.4 Å). For 405D, the most populated clusters are 1.15 Å apart, but we cannot find a clear correspondence between other clusters. This is the system with the most variability, as reflected through both sets of simulations.

Grooves Analysis. Using Curves++ and Canal,⁴⁸ we performed an analysis of the groove widths for atomistic simulations using the crystal and the reconstructed structures. The minor groove widths, although varying for the different systems, do not exhibit large variations, and are nearly identical between simulations from the crystal and reconstructed structures. The major groove widths, presented in Figure 12, show much larger variations, although the values stay similar between crystal and reconstructed structure. For the two RNA systems, the values are well in the range of the usual values for RNAs (one should note that the values for groove width calculated by Curves++ are decreased by 5.8 Å, to take into account the van der Waals surface from the backbone). For 433D, the major groove width from the starting simulation is among the lower values observed during the simulation. The values sampled during our simulations fall in the range of values present in NMR structures, with X-ray structures generally having narrower major grooves, as presented in ref 49.

Comparison of 433D and 433Dsym. Using atomistic simulations, we can detail the structural differences of 433D and 433Dsym. For 433D, we considered the experimental structure, while, for 433Dsym, we used the reconstruction

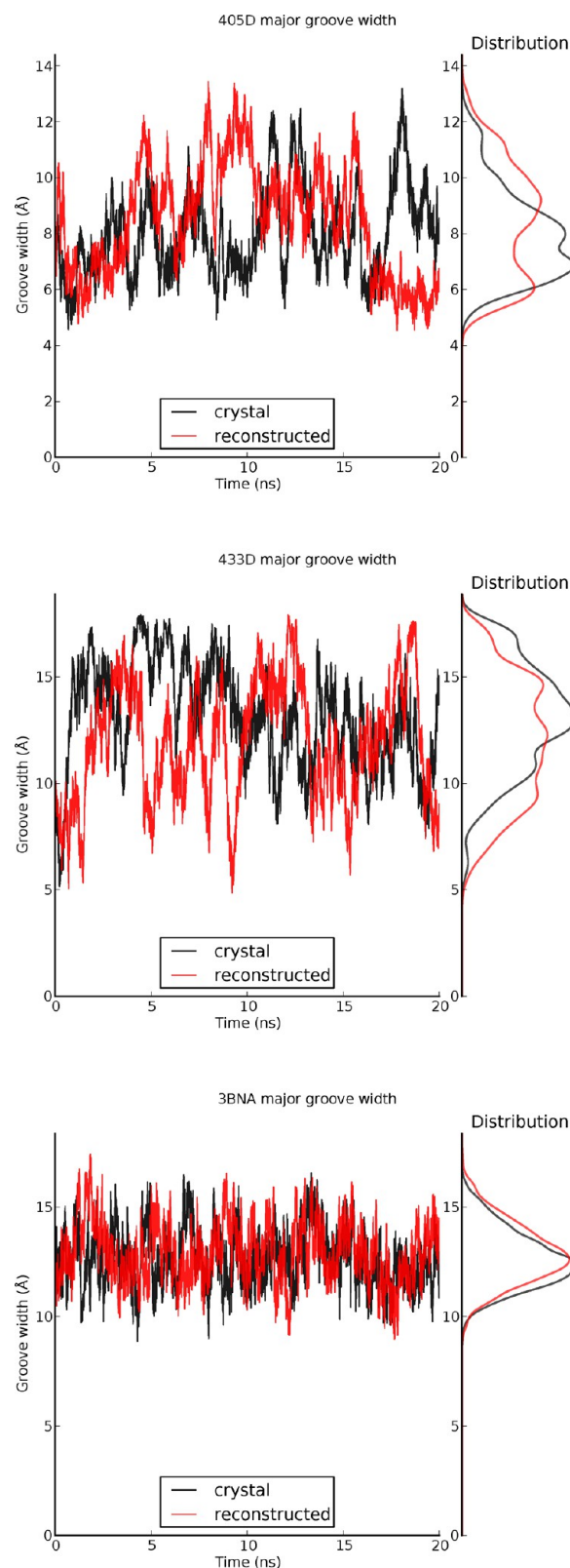


Figure 12. Time series evolution and distribution of the major grooves.

procedure from a low temperature cluster of the REMD, followed by an atomistic simulation using the protocol just described. We take as a reference structure that of the most populated cluster. From the structure superposition, we observe that the ends of the molecules are very well aligned, while both

bases and backbone adopt a different shape in the central region, where the sequence is different (Figure 13). The RMSD

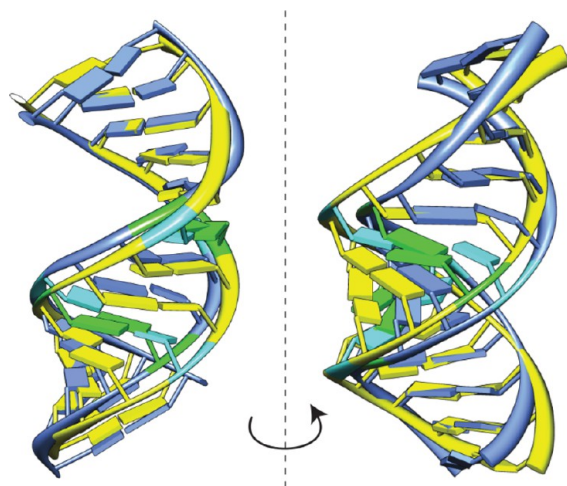


Figure 13. Comparison of 433D (blue) and 433DU (yellow) at atomic resolution.

of the two molecules is 2.4 Å. We can further quantify their discrepancy looking at the dihedral angles. We have taken as a reference the average values of the dihedral angles in a regular A RNA helix, as given in ref 27, and compared all dihedrals of all bases to those of the standard helix. As a reference, the variability of the angles forming canonical WC pairings averages between 5 and 10° and it can be as high as 20°. Both systems exhibit large discrepancies for some of the bases involved in the mismatch. If we look at the first strand, for 433D, the G9 has a value of α and γ deviating by more than 100° with respect to the standard values (α , +130; γ , -116). G10, on the other hand, lies in the range of the standard A-helix, and the same is true for the two U bases involved in the other mismatch (U5 and U6). Similar values are adopted by the mismatching G bases of the second strand.

For 433Dsym, the G10 exhibits a significant variation of the dihedral angle β (β , -40), and slightly different values for α and ϵ (α , +27; ϵ , +24). U11 exhibits the largest differences with respect to the standard A-helix, with deviations of α = +145 and γ = -140. This system is asymmetric with respect to the two strands, as there is no significant deformation of the second strand on any base.

CONCLUSIONS

The study of large conformational changes in nucleic acids, such as folding or assembly, remains an open challenge in the computational field because of the large size of the molecules and of the long time scales on which such transitions occur. At the time being, the only viable path to approach sizable nucleic acid systems is a drastic reduction of the degrees of freedom that are considered. The choice of what to retain in the model largely depends on the biological questions one wants to address. This explains the existence of several coarse-grained models for RNA and DNA, each one with its own peculiarities both in the type of representation adopted and in the force fields implemented.

In this work, we have presented a new application of our high resolution, fully flexible model for RNA and DNA. A specific feature of our model is the high resolution of the nucleotides, that we represent with six or seven beads, instead of two or

three like in most other models. This degree of accuracy in the geometrical description allows us to have a system in which we do not have to impose constraints to hold the molecule in native-like conformations, and makes our model suitable for studies of folding and assembly. All configurations can be explored, even if they depart significantly from the regular double helix and the canonical Watson–Creek pairing. However, the reduction is still very significant and allows us to perform simulations in which we can indeed observe large conformational changes. As we have shown here as a proof of principles, with our model, we can investigate both dynamical and thermodynamical aspects of double helical assemblies. We can compare the thermodynamics of molecules with the same base composition, but with different sequences, and investigate the effect of sequences on the melting curves of the duplexes. This result opens to the possibility of more detailed studies in which the sequence dependence of the thermodynamical and dynamical behavior can be studied systematically.

No matter the model, when adopting a coarse-grained approach, there is always a level of detail that is lost. We have developed a reconstruction algorithm to convert coarse-grained structures back to full atomistic details. This reversion is easily feasible in our model thanks to the high level of resolution we adopt and because the nucleotides are relatively rigid objects: such reconstruction would not have been so successful had we adopted a more reduced model of two or three beads only. We have shown here that atomistic simulations starting from experimental structures or from structures reconstructed from coarse-grained molecules are substantially equivalent. This validates the possibility, for molecules for which an experimental structure is not known, to use a coarse-grained representation and to run (RE)MD simulations from an arbitrary configuration to obtain a low temperature stable structure, and then, after atomistic reconstruction, use the power of atomistic simulations to investigate all details, once the heavy duty job of folding or assembly has been carried out by the coarse-grained model.

One of the main limitations of our model is the absence of a description for ions. We are currently investigating various options to incorporate those molecules in a future development. For the work presented here concerning duplexes, the limitation is less severe than for large molecules. In extended double helices, ions are regularly distributed inside the grooves and though providing a screening for the phosphate negative charges, they do not usually play a structural role. On the other hand, for large molecules with complex architectures, ions are found in very specific positions and are essential in stabilizing the structure. As we want to address these large molecules, an explicit description of ions is unavoidable. It is relevant to point out that even atomistic models have difficulties in treating ions, and that the questions on how to properly model them is a more general issue than just for coarse-grained models.

Our coarse-grained model still needs to be optimized in its parameters and functional form (to include explicit stacking potentials, for example). Therefore, our results, which illustrate the potential and versatility of the CG model, should not be considered accurate in their quantitative details. In particular, the exact correspondence between our temperature scale and real temperatures still needs to be drawn. For this purpose, we now have an ongoing collaboration with experimentalists to provide us with data directly comparable to our simulation results. When drawing a direct correspondence between simulations and experiments, particular care needs to be

taken to include finite-size effects of dilution of an isolated simulated duplex with respect to real bulk experiments.^{50,51} These corrections will also be taken into account. As a final remark, it should be noticed that the need for further refinement is also true of DNA and RNA atomistic models, where the force fields are in continuous development.^{23,52–54}

■ ASSOCIATED CONTENT

● Supporting Information

Description of the full details of the model. This material is available free of charge via the Internet at <http://pubs.acs.org>.

■ AUTHOR INFORMATION

Corresponding Author

*E-mail: samuella.pasquali@ibpc.fr. Phone: +33-1-58415169.

Notes

The authors declare no competing financial interest.

■ ACKNOWLEDGMENTS

The authors wish to thank the Ecole Doctorale B3MI for the financial support of T.C. and the CASPUR computing facility in Rome, where all atomistic simulations have been performed. Support for this work has also been provided by the French government grant ANR-11-LABEX-0011-01.

■ REFERENCES

- (1) Djebali, S.; Davis, C. a.; Merkel, A.; Dobin, A.; Lassmann, T.; Mortazavi, A.; Tanzer, A.; Lagarde, J.; Lin, W.; Schlesinger, F.; Xue, C.; Marinov, G. K.; Khatun, J.; Williams, B. a.; Zaleski, C.; et al. Landscape of Transcription in Human Cells. *Nature* **2012**, *489*, 101–108.
- (2) Guttman, M.; Amit, I.; Garber, M.; French, C.; Lin, M. F.; Feldser, D.; Huarte, M.; Zuk, O.; Carey, B. W.; Cassady, J. P.; Cabili, M. N.; Jaenisch, R.; Mikkelsen, T. S.; Jacks, T.; Hacohen, N.; et al. Chromatin Signature Reveals over a Thousand Highly Conserved Large Non-Coding RNAs in Mammals. *Nature* **2009**, *458*, 223–227.
- (3) Cruz, J. A.; Westhof, E. The Dynamic Landscapes of RNA Architecture. *Cell* **2009**, *136*, 604–609.
- (4) Ponting, C. P.; Oliver, P. L.; Reik, W. Evolution and Functions of Long Noncoding RNAs. *Cell* **2009**, *136*, 629–641.
- (5) Wilusz, J. E.; Sunwoo, H.; Spector, D. L. Long Noncoding RNAs: Functional Surprises from the RNA World. *Genes Dev.* **2009**, *23*, 1494–1504.
- (6) Reiter, N. J.; Chan, C. W.; Mondragón, A. Emerging Structural Themes in Large RNA Molecules. *Curr. Opin. Struct. Biol.* **2011**, *1*–8.
- (7) Li, P. T. X.; Viereg, J.; Tinoco, I. How RNA Unfolds and Refolds. *Annu. Rev. Biochem.* **2008**, *77*, 77–100.
- (8) Woodson, S. a. Compact Intermediates in RNA Folding. *Annu. Rev. Biophys.* **2010**, *39*, 61–77.
- (9) Sim, A. Y. L.; Minary, P.; Levitt, M. Modeling Nucleic Acids. *Curr. Opin. Struct. Biol.* **2012**, *22*, 273–278.
- (10) Bowman, G. R.; Huang, X.; Yao, Y.; Sun, J.; Carlsson, G.; Guibas, L. J.; Pande, V. S. Structural Insight into RNA Hairpin Folding Intermediates. *J. Am. Chem. Soc.* **2008**, *130*, 9676–9678.
- (11) Hyeon, C.; Thirumalai, D. Capturing the Essence of Folding and Functions of Biomolecules Using Coarse-Grained Models. *Nat. Commun.* **2011**, *2*, 487.
- (12) Xayaphoummine, a.; Bucher, T.; Isambert, H. Kinefold Web Server for RNA/DNA Folding Path and Structure Prediction Including Pseudoknots and Knots. *Nucleic Acids Res.* **2005**, *33*, W605–W610.
- (13) Cao, S.; Chen, S.-J. Predicting RNA Folding Thermodynamics with a Reduced Chain Representation Model. *RNA* **2005**, *11*, 1884–1897.
- (14) Bernauer, J.; Huang, X.; Sim, A. Y. L.; Levitt, M. Fully Differentiable Coarse-Grained and All-Atom Knowledge-Based Potentials for RNA Structure Evaluation. *RNA* **2011**, *17*, 1066–1075.
- (15) Sharma, S.; Ding, F.; Dokholyan, N. V. iFoldRNA: Three-Dimensional RNA Structure Prediction and Folding. *Bioinformatics* **2008**, *24*, 1951–1952.
- (16) Jonikas, M. a.; Radmer, R. J.; Laederach, A.; Das, R.; Pearlman, S.; Herschlag, D.; Altman, R. B. Coarse-Grained Modeling of Large RNA Molecules with Knowledge-Based Potentials and Structural Filters. *RNA* **2009**, *15*, 189–199.
- (17) Morriss-Andrews, A.; Rottler, J.; Plotkin, S. S. A Systematically Coarse-Grained Model for DNA and Its Predictions for Persistence Length, Stacking, Twist, and Chirality. *J. Chem. Phys.* **2010**, *132*, 035105.
- (18) Ouldridge, T. E.; Louis, A. a.; Doye, J. P. K. Structural, Mechanical, and Thermodynamic Properties of a Coarse-Grained DNA Model. *J. Chem. Phys.* **2011**, *134*, 085101.
- (19) Dans, P. D.; Zeida, A.; Machado, M. R.; Pantano, S. A Coarse Grained Model for Atomic-Detailed DNA Simulations with Explicit Electrostatics. *J. Chem. Theory Comput.* **2010**, *6*, 1711–1725.
- (20) Poulain, P.; Saladin, A.; Hartmann, B.; Prévost, C. Insights on Protein-DNA Recognition by Coarse Grain Modelling. *J. Comput. Chem.* **2008**, *29*, 2582–2592.
- (21) Hsu, C. W.; Fyta, M.; Lakatos, G.; Melchionna, S.; Kaxiras, E. Ab Initio Determination of Coarse-Grained Interactions in Double-Stranded DNA. *J. Chem. Phys.* **2012**, *137*, 105102.
- (22) Pasquali, S.; Derreumaux, P. HiRE-RNA: a High Resolution Coarse-Grained Energy Model for RNA. *J. Phys. Chem. B* **2010**, *114*, 11957–11966.
- (23) Krepl, M.; Zgarbová, M.; Stadlbauer, P.; Otyepka, M.; Banáš, P.; Koča, J.; Cheatham, T. E.; Jurečka, P.; Sponer, J. Reference Simulations of Noncanonical Nucleic Acids with Different χ Variants of the AMBER Force Field: Quadruplex DNA, Quadruplex RNA and Z-DNA. *J. Chem. Theory Comput.* **2012**, *8*, 2506–2520.
- (24) Sponer, J.; Riley, K. E.; Hobza, P. Nature and Magnitude of Aromatic Stacking of Nucleic Acid Bases. *Phys. Chem. Chem. Phys.* **2008**, *10*, 2595–2610.
- (25) Holbrook, S. R. Structural Principles from Large RNAs. *Annu. Rev. Biophys.* **2008**, *37*, 445–464.
- (26) Lindorff-Larsen, K.; Piana, S.; Dror, R. O.; Shaw, D. E. How Fast-Folding Proteins Fold. *Science* **2011**, *334*, 517–520.
- (27) Richardson, J. S.; et al. RNA Backbone: Consensus All-Angle Conformers and Modular String Nomenclature (an RNA Ontology Consortium Contribution). *RNA* **2008**, *14*, 465–481.
- (28) Berman, H. M.; Olson, W. K.; Beveridge, D. L.; Westbrook, J.; Gelbin, a.; Demeny, T.; Hsieh, S. H.; Srinivasan, a. R.; Schneider, B. The Nucleic Acid Database. A Comprehensive Relational Database of Three-Dimensional Structures of Nucleic Acids. *Biophys. J.* **1992**, *63*, 751–759.
- (29) Parsons, J.; Holmes, J. B.; Rojas, J. M.; Tsai, J.; Strauss, C. E. M. Practical Conversion from Torsion Space to Cartesian Space for In Silico Protein Synthesis. *J. Comput. Chem.* **2005**, *26*, 1063–1068.
- (30) Heath, A. P.; Kavraki, L. E.; Clementi, C. From Coarse-Grain to All-Atom: Toward Multiscale Analysis of Protein Landscapes. *Proteins* **2007**, *68*, 646–661.
- (31) Rzeplia, A. J.; Schäfer, L. V.; Goga, N.; Risselada, H. J.; De Vries, A. H.; Marrink, S. J. Reconstruction of Atomistic Details from Coarse-Grained Structures. *J. Comput. Chem.* **2010**, *31*, 1333–1343.
- (32) Pan, B.; Mitra, S. N.; Sundaralingam, M. Structure of a 16-mer RNA Duplex r(GCAGACUAAAUCUGC)₂ with Wobble C.A+ Mismatches. *J. Mol. Biol.* **1998**, *283*, 977–984.
- (33) Trikha, J.; Filman, D. J.; Hogle, J. M. Crystal Structure of a 14 bp RNA Duplex with Non-Symmetrical Tandem GxU Wobble Base Pairs. *Nucleic Acids Res.* **1999**, *27*, 1728–1739.
- (34) Gautheret, D.; Konings, D.; Gutell, R. R. G.U Base Pairing Motifs in Ribosomal RNA. *RNA* **1995**, *1*, 807–814.
- (35) Xia, T.; McDowell, J. A.; Turner, D. H. Thermodynamics of Nonsymmetric Tandem Mismatches Adjacent to G.C Base Pairs in RNA. *Biochemistry* **1997**, *36*, 12486–12497.
- (36) Fratini, A. V.; Kopka, M. L.; Drew, H. R.; Dickerson, R. E. Reversible Bending and Helix Geometry in a B-DNA Dodecamer: CGCGAATTBrCGCG. *J. Biol. Chem.* **1982**, *257*, 14686–14707.

- (37) Chebaro, Y.; Mousseau, N.; Derreumaux, P. Structures and Thermodynamics of Alzheimer's Amyloid-Beta Abeta(16–35) Monomer and Dimer by Replica Exchange Molecular Dynamics Simulations: Implication for Full-Length Abeta Fibrillation. *J. Phys. Chem. B* **2009**, *113*, 7668–7675.
- (38) Spill, Y. G.; Pasquali, S.; Derreumaux, P. Impact of Thermostats on Folding and Aggregation Properties of Peptides Using the Optimized Potential for Efficient Structure Prediction Coarse-Grained Model. *J. Chem. Theory Comput.* **2011**, *7*, 1502–1510.
- (39) Derreumaux, P.; Mousseau, N. Coarse-Grained Protein Molecular Dynamics Simulations. *J. Chem. Phys.* **2007**, *126*, 025101.
- (40) Chodera, J. D.; Swope, W. C.; Pitera, J. W.; Seok, C.; Dill, K. A. Use of the Weighted Histogram Analysis Method for the Analysis of Simulated and Parallel Tempering Simulations. *J. Chem. Theory Comput.* **2007**, *3*, 26–41.
- (41) Salim, N.; Lamichhane, R.; Zhao, R.; Banerjee, T.; Philip, J.; Rueda, D.; Feig, A. L. Thermodynamic and Kinetic Analysis of an RNA Kissing Interaction and Its Resolution into an Extended Duplex. *Biophys. J.* **2012**, *102*, 1097–1107.
- (42) SantaLucia, J., Jr. A Unified View of Polymer, Dumbbell, and Oligonucleotide DNA Nearest-Neighbor Thermodynamics. *Proc. Natl. Acad. Sci. U.S.A.* **1998**, *95*, 1460–1465.
- (43) Peyret, N.; Seneviratne, P. A.; Allawi, H. T.; SantaLucia, J., Jr. Nearest-Neighbor Thermodynamics and NMR of DNA Sequences with Internal A.A, C.C, G.G, and T.T Mismatches. *Biochemistry* **1999**, *38*, 3468–3477.
- (44) Humphrey, W.; Dalke, A.; Schulten, K. VMD: Visual Molecular Dynamics. *J. Mol. Graphics* **1996**, *14* (33–8), 27–28.
- (45) Hess, B.; Kutzner, C.; van der Spoel, D.; Lindahl, E. GROMACS 4: Algorithms for Highly Efficient, Load-Balanced, and Scalable Molecular Simulation. *J. Chem. Theory Comput.* **2008**, *4*, 435–447.
- (46) Pérez, A.; Marchán, I.; Svozil, D.; Spöner, J.; Cheatham, T. E.; Laughton, C. a.; Orozco, M. Refinement of the AMBER Force Field for Nucleic Acids: Improving the Description of Alpha/Gamma Conformers. *Biophys. J.* **2007**, *92*, 3817–3829.
- (47) Jorgensen, W. L.; Chandrasekhar, J.; Madura, J. D.; Impey, R. W.; Klein, M. L. Comparison of Simple Potential Functions for Simulating Liquid Water. *J. Chem. Phys.* **1983**, *79*, 926.
- (48) Lavery, R.; Moakher, M.; Maddocks, J. H.; Petkeviciute, D.; Zakrzewska, K. Conformational Analysis of Nucleic Acids Revisited: Curves+. *Nucleic Acids Res.* **2009**, *37*, 5917–5929.
- (49) Tolbert, B. S.; Miyazaki, Y.; Barton, S.; Kinde, B.; Starck, P.; Singh, R.; Bax, A.; Case, D. a.; Summers, M. F. Major Groove Width Variations in RNA Structures Determined by NMR and Impact of ¹³C Residual Chemical Shift Anisotropy and ¹H-¹³C Residual Dipolar Coupling on Refinement. *J. Biomol. NMR* **2010**, *47*, 205–219.
- (50) Ouldridge, T. E.; Louis, A. a.; Doye, J. P. K. Extracting Bulk Properties of Self-Assembling Systems from Small Simulations. *J. Phys.: Condens. Matter* **2010**, *22*, 104102.
- (51) Ouldridge, T. E. Inferring Bulk Self-Assembly Properties from Simulations of Small Systems with Multiple Constituent Species and Small Systems in the Grand Canonical Ensemble. *J. Chem. Phys.* **2012**, *137*, 144105.
- (52) Lagant, P.; Derreumaux, P.; Vergoten, G.; Peticolas, W. The Use of Ultraviolet Resonance Raman Intensities to Test Proposed Molecular Force Fields for Nucleic Acid Bases. *J. Comput. Chem.* **1991**, *12*, 731–741.
- (53) Yildirim, I.; Kennedy, S. D.; Stern, H. a.; Hart, J. M.; Kierzek, R.; Turner, D. H. Revision of AMBER Torsional Parameters for RNA Improves Free Energy Predictions for Tetramer Duplexes with GC and iG/C Base Pairs. *J. Chem. Theory Comput.* **2012**, *8*, 172–181.
- (54) Hart, K.; Foloppe, N.; Baker, C. M.; Denning, E. J.; Nilsson, L.; MacKerell, A. D. Optimization of the CHARMM Additive Force Field for DNA: Improved Treatment of the BI/BII Conformational Equilibrium. *J. Chem. Theory Comput.* **2012**, *8*, 348–362.